Lifetime of THz Acoustic Nanocavity Modes

G. Rozas,[1] M. F. Pascual Winter,[1,2] B. Jusserand,[2] A. Fainstein,[1,*] B. Perrin,[2] E. Semenova,[3] and A. Lemaître[3]

[1]*Centro Atómico Bariloche & Instituto Balseiro, CNEA, Bustillo 9500, R8402AGP S. C. de Bariloche, Río Negro, Argentina*

[2]*Institut des Nanosciences de Paris, Université Pierre et Marie Curie, CNRS UMR 7588, Campus Boucicaut, 140 Rue de Lourmel, 75015 Paris, France*

[3]*Laboratoire de Photonique et de Nanostructures, CNRS, Route de Nozay, 91460 Marcoussis, France*

(Received 7 August 2008; published 5 January 2009)

We present an ultrahigh resolution Raman study of the lifetime of 1 THz acoustic phonons confined in nanocavities. We demonstrate that the cavity Q factor can be controlled by design. Anharmonicity contributes only marginally to limit the cavity phonon lifetime, even at room temperature, while thickness fluctuations in the scale of $1/10$ of a unit cell are the main limitation for the performance of THz phonon cavities.

DOI: 10.1103/PhysRevLett.102.015502 PACS numbers: 63.22.Np, 62.80.+f, 78.30.Fs

Phonons in the THz range have great importance both in basic research and in applications, for example, in optoelectronics or nanoscopy [1–3]. One important device in this area is the phonon cavity [4]. Being a monochromatic source for large strains, its potential applications include studies of crystal dynamics above the elastic regime [5] and sources for coherent phonon generation [2,6] and control [7]. However, several fundamental limitations to the performance of these THz cavities that are intrinsic to acoustic phonons, and become critical at the interesting room-temperature, high-frequency, and nanometer-wavelength regime, have not been tested so far. By means of a newly developed ultrahigh resolution Raman scattering technique, we show that we can control by design the intrinsic lifetime of 1 THz phonon cavities. The effects of anharmonicity and thickness fluctuations are addressed through temperature-dependent measurements and Raman scattering simulations.

The phonon cavity is the acoustic equivalent of the photon cavity [8]. It consists of a spacer of width $n\frac{\lambda}{2}$ enclosed between two superlattices (SL). Because of the acoustic impedance mismatch between the materials, the latter act as interference acoustic mirrors [9,10] for the wavelength λ. Like its photonic counterpart, phonon cavities are characterized by a highly monochromatic and amplified acoustic mode, with sound wavelengths of the order of a few nanometers [4]. The quality of the cavity is given by its Q factor $Q = \lambda/\Delta\lambda$, where $\Delta\lambda$ is the full-width at half-maximum (FWHM) of the cavity mode. The theoretical Q factor can be controlled through the reflectivity of the acoustic mirrors, being larger for higher reflectivities. It is also closely related to the lifetime of the cavity phonons, which live longer in the cavity region as the reflectivity of the mirrors increases. For example, for a 1 THz phonon ($\lambda \sim 5$ nm in GaAs), a Q factor of 10^4 implies a lifetime of $\sim$3 ns, which should be compared to the $\sim$2 ps it takes a nonconfined vibration to go through the cavity spacer. Such lifetime can be achieved in principle with mirrors of only 20 GaAs/AlAs bilayers.

However, in spite of their many similarities, there are two crucial differences between photonic and acoustic cavities. First, photons are intrinsically harmonic: they do not decay unless they interact with a nonlinear material. Phonons, in contrast, are intrinsically anharmonic [11,12]. A phonon will always decay into two or more phonons or will collide with a phonon present in the thermal bath, their lifetime being a direct consequence of the nonparabolicity of the lattice atomic potential [12,13]. Second, while mirrors with surface qualities of $\lambda_{\text{light}}/200$ for light in the visible and near-infrared can be obtained, the equivalent quality for phonons of $\lambda \sim 5$ nm would be challenging even for the best state-of-the-art MBE, leading to a possible strong interaction of phonons with surface imperfections in most of the structures. Several experimental and theoretical reports in the area of thermal conductivity of nanostructures show that both the bulk phonon lifetime and the scattering at interfaces and defects should be taken into account to properly approach the problem [14,15]. The practical limitations to the lifetime and consequently to the minimum linewidth and maximum amplification that can be achieved in these cavities are important matters for device applications. In addition, the anharmonic phonon decay is in itself a challenging fundamental issue, both experimentally and theoretically [16–18]. The lifetime of propagating THz acoustic phonons both in bulk and in nanostructures, which are at the heart of the current developments in picosecond acoustics, remains an open problem that can be addressed by the method reported here.

Four acoustic cavities [4] with a mode frequency of 1 THz were grown by MBE on top of an optical mirror [Fig. 1(a)], so that the full sample acts as an optical microcavity [19]. Each acoustic cavity is formed by a top 20-period GaAs/AlAs (3.5/1.5 nm) SL, a $\frac{3\lambda}{2}$ GaAs spacer (7 nm), and a bottom SL mirror with $N = 4$, 8, 12, or 16 similar periods depending on the sample. This introduces a variation in the reflectivity of the bottom mirror (from 36% to 98.5%) that, in turn, modifies the Q factor of the acoustic cavity (from 63 to 2400). The optical mirror is an

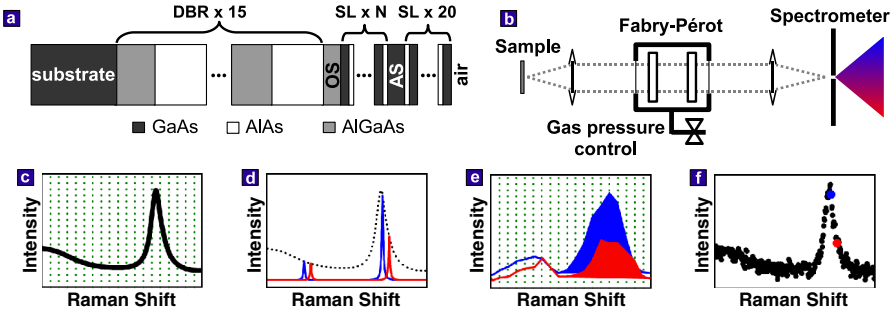

FIG. 1 (color online). Scheme of the samples (a) and experimental setup (b). AS and SL (OS and DBR) stand for acoustic (optic) spacer and mirror. Panel (c) shows how the Raman spectrum (full line) compares to the CCD pixel size (delimited by vertical dotted lines in c and e) in a typical experimental condition. Panels (d)–(f) represent the different stages in the reconstruction of the Raman spectrum (see the text for details). The two full-line spectra correspond to two different gas pressures, and each shaded area correspond to one point in the final spectrum. The four panels have the same full bottom scale of 1.7 cm^{-1}.

$AlAs/Al_{0.33}Ga_{0.67}As$ DBR centered at 750 nm. A sample dependent $Al_{0.33}Ga_{0.67}As$ layer was grown between this mirror and the bottom of the acoustic SL to produce a λ_{laser} optical spacer between the air and the DBR, and to assure that the acoustic cavity spacer is at a maximum of the amplified electric field independently of N. The presence of the optical microcavity has a twofold purpose: increasing the Raman signal, and enabling the detection in a backscattering geometry of the cavity peak, otherwise accessible only in a forward-scattering configuration [4,20]. Both the AlGaAs layer and the DBR (but not the acoustic nanocavity) were grown with a ~15% wedge to allow for the tuning of the optical cavity to the electronic resonance of the SL, further increasing the Raman signal. Room-temperature photoluminescence shows that all the samples have their SL fundamental emission between 751 and 754 nm, and that the DBRs do not absorb at wavelengths larger than 670 nm.

The mentioned Q factors mean that the cavity mode tunnels through the bottom SL to the substrate at lifetimes that vary from 20 to 790 ps for the 4- and 16-period samples, respectively. To test these nominal values, we use the close relationship between the lifetime of the cavity mode and the linewidth of the Raman scattering peak. If the former is τ, then the latter will be FWHM $= 2\hbar/\tau$. The expected Raman linewidths for the cavity mode vary then from 0.52 to 0.014 cm^{-1}. This sets the resolution needed for Raman experiments on these samples well below the capabilities of a high resolution triple Raman spectrometer in the additive configuration (~ 0.2 cm^{-1} in the near-infrared, NIR). On the other hand, a Fabry-Pérot (FP)–spectrometer tandem with monochannel acquisition [21] could provide the required resolution but with acquisition times that would be prohibitive in the present samples. In order to overcome these difficulties, we have developed a novel Fabry-Pérot–triple additive spectrometer tandem with multichannel acquisition [Fig. 1(b)]. In this setup, the light coming from the experiment [1(c)] goes through a single-pass FP interferometer (97% NIR dielectric mirrors) and gets multiplied by its transmission function [1(d)]. This function consists of a series of narrow transmission peaks equally spaced (being this distance the free spectral range, FSR) that can be tuned by changing the pressure and, consequently, the index of refraction of the gas in the interior of the FP. This filtered light is collected later into a Dilor XY800 triple spectrometer in additive configuration and acquired with a liquid nitrogen-cooled CCD. As the resolution of the spectrometer is better than the FSR of the FP but not enough to resolve the width of the transmission peaks, the acquired spectrum consists of several broad resolution-limited peaks of which the relevant information is their integrated intensity [1(e)]. Repeating this procedure as a function of the gas pressure, we reconstruct the Raman profile [1(f)]. This configuration allows to acquire a full 10 cm^{-1} Raman spectrum with the ultrahigh resolution characteristic of a FP interferometer (0.01 cm^{-1}) in only one simultaneous parallel measurement.

The experiments were performed in backscattering, with 1 mW power focused in an 80 μm spot and with the laser energy 10 meV below the SL gap. The optical microcavity mode was tuned by displacing the sample to obtain maximum Raman signal. The laser was a tunable Ti:Saph with a measured linewidth of 0.013 cm^{-1} (390 MHz, Fig. 2). Typical acquisition time for one spectrum was 1–3 hours.

Room-temperature Raman measurements are presented in Fig. 2. Vertical arrows identify the acoustic cavity peak. The $q = 0$ (“forward”-scattering, FS) and $q = 2k$ (“back”-scattering, BS) modes of the SLs, where q (k) is the phonon (photon) wave vector, are also identified. As expected from the design, all samples have the cavity mode around 33 cm^{-1} (~ 1 THz), and it is in all cases less than 0.1 cm^{-1} away from the predicted position based on x-ray data for the layers widths. Calculations of Raman scattering spectra [22] were performed to compare the experimental linewidths with those expected for samples without any additional broadening [Fig. 2(b)]. While the theoretical linewidth (full line) decreases exponentially with the number of periods of the bottom SL, the experimental linewidth (full circles) saturates towards a value of ~0.1 cm^{-1}

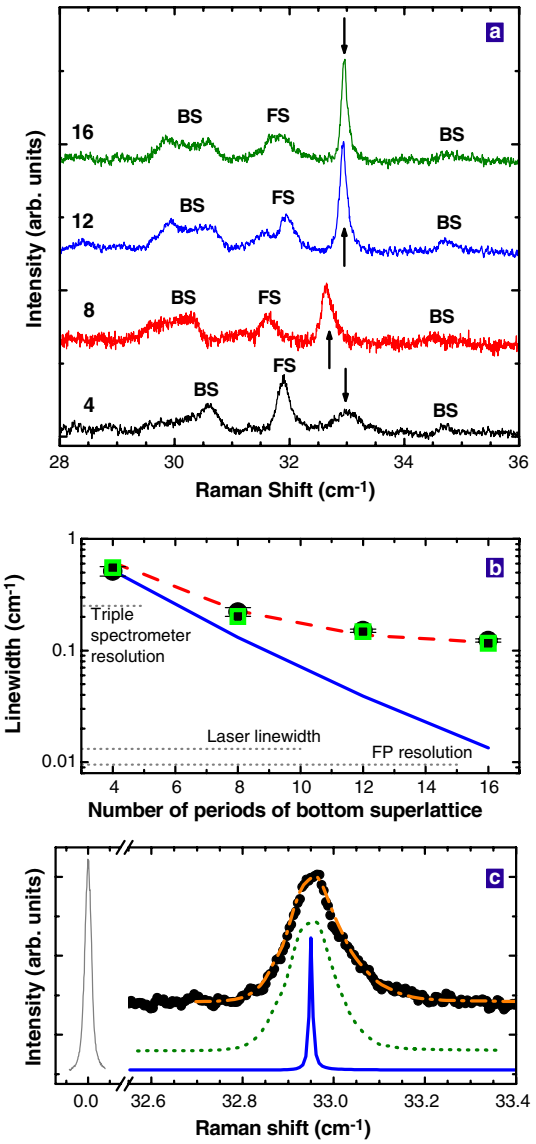

FIG. 2 (color online). (a) Room-temperature ultrahigh resolution Raman spectra of the four samples, identified by the number of periods of the bottom SL. Vertical arrows mark the acoustic cavity mode. Panels (b), (c) show a comparison of experimental (full circles) and calculated nominal (full line), Lorentzian convoluted (dashed line), thickness fluctuations (empty squares and dotted line), and thickness fluctuations with wave vector relaxation (dash-dotted line) linewidths and profiles of the acoustic cavity mode Raman peak. Both Lorentzian convolution and thickness fluctuations are also convoluted with the experimental resolution. In panel (c), the three theoretical spectra are shifted $+0.07\ \mathrm{cm}^{-1}$ to match the experimental position of the peak. Laser profile (thin full line) is also shown.

(which would correspond, if it were homogeneous, to a 110 ps lifetime). Several resolution limits are also plotted for reference. For the 16-period sample, we compare in Fig. 2(c) the room-temperature experimental (full circles) and theoretical (full line) Raman spectra, the former being 8 times broader. The measured laser line (thin full line) is presented as well as a reference of the resolution of the tandem. A Lorentzian convolution of FWHM $= 0.1\ \mathrm{cm}^{-1}$ of the theoretical spectra matches very well the general behavior seen in Fig. 2(b) (dashed line). The dependence of the FWHM with the size of the bottom SL shows that, through a proper design of the sample, it is possible to modify the Q factor and lifetime of the acoustic cavity.

For the lowest Q 4-period acoustic cavity, the experimental linewidth is consistent with that expected from theory. However, it is clear from the other samples that an additional broadening mechanism is present. As we mentioned earlier, phonons are subject to anharmonic decay. This mechanism strongly depends on temperature and energy because high-energy phonons have more chances to decay into lower-energy phonons, and thermally-excited populations can stimulate this decay [12,13]. To identify the relative contribution of this mechanism, we have performed temperature-dependent Raman scattering experiments, shown in Fig. 3 for the 16-period sample. The experimental linewidth of the cavity peak does not change significantly when we reduce the temperature from 293 to 135 K. The anharmonic decay rate is proportional to the phonon population at the final states [11,12]. At relatively high temperatures, i.e., when $\hbar\omega < kT \lesssim kT_{\mathrm{Debye}}$, phonon population is proportional to the temperature T, and anharmonic lifetime can be approximated as $\tau_{\mathrm{anh}}^{-1} = \Gamma\omega^2 T$, $\hbar\omega$ being the energy of the initial phonon and Γ a constant that depends on the anharmonicity of the interatomic forces, if only three-phonon Herring processes are taken into account [12,13]. For reference, phonon frequencies around 1 THz are equivalent to $\sim$50 K, and $T_{\mathrm{Debye}} =$ 344 K for GaAs. If anharmonic decay were the main contribution to the broadening, this should lead to a twofold reduction of the linewidth, which is clearly not the case. The experimental reduction in this temperature range

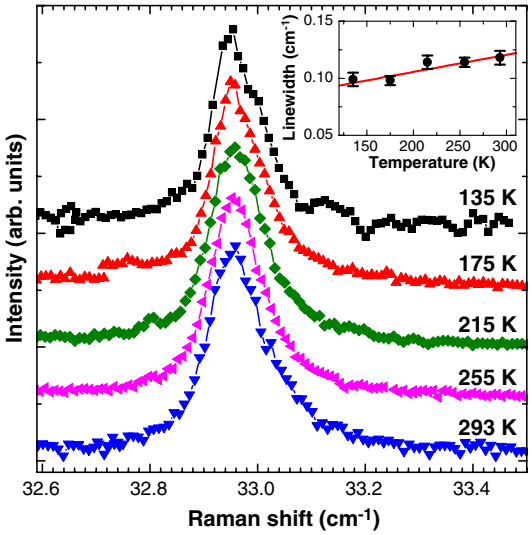

FIG. 3 (color online). Temperature dependence of the acoustic cavity mode Raman peak for the sample with 16 periods in the bottom superlattice. The inset shows the FWHM of this peak (full circles) fitted by a linear temperature dependence (full line).

is (0.019 ± 0.008) cm^{-1} and amounts only to 15% of the total linewidth. We can estimate Γ proposing that the Raman line profile is the convolution of a temperature independent peak of width W_0 and the anharmonic broadening $W_A = 2\hbar/\tau_{\mathrm{anh}}$. Fitting this temperature dependence with $\omega/(2\pi) = \nu_{\mathrm{cav}} = 1$ THz to the experimental points results in $\Gamma = (3.6 \pm 1.0) \times 10^{-19}$ K^{-1} s (solid line in the inset). In order to obtain a theoretical estimation of this parameter, we can write $\Gamma = 2\upsilon A'$, where $\upsilon = 4950$ m/s is the effective sound velocity in the system and A' is the parameter defined in equation (10) of Ref. [13], calculated to be 1.1×10^{-25} cm^{-1} s^2 K^{-1} for bulk GaAs in the same reference. This sets $\Gamma = 1.1 \times 10^{-19}$ K^{-1} s, in good agreement with our experimental value, and supports the prediction by Chen *et al.* [13] that Herring scattering should dominate over the relaxation process for frequencies above 500 GHz. The existent discrepancy in the values can have several origins: (i) bulk momentum conservation is modified in a SL by the folding of the dispersion relationship, opening new channels for umklapp processes [14]; (ii) we are dealing here with a localized mode, for which momentum conservation is relaxed [23].

Excluded anharmonic decay as the main contribution, the other possible sources of broadening for phonons in nanostructures are deviations from the ideal system, namely, scattering on roughness at interfaces and material mixing. As they are produced by fixed properties of the structure, these factors should be temperature independent. Besides, thickness fluctuations can have large consequences. Even if small variations in the layers widths do not affect significantly the linewidth of the cavity mode, the small energy shift produced by the different local parameters at each point of the sample can cause an inhomogeneous broadening of the Raman peak. To test the latter, we have performed Raman scattering calculations introducing a random variation in the position of the interfaces. Using an exponential random distribution with probability $p(\delta) = \exp(-|\frac{\delta}{\alpha}|)/(2\alpha)$ for the deviation δ from the expected position of each interface, we have concluded that fluctuations of 1/9 of a unit cell ($\alpha = 0.06$ nm) can reproduce the experimental results for all the samples [empty squares in Fig. 2(b)]. As an example, we plot in Fig. 2(c) the average spectrum for 3000 random samples (dotted line) simulated with this α parameter and taking δ as deviations from the x-ray values. α in this 1D simulation can be seen as an average sensed by the phonon of the short range roughness typical of the GaAs-over-AlAs interfaces [24]. The observed slight peak asymmetry with a high-energy tail can be accounted for by including momentum relaxation as described in Ref. [25], in addition to the symmetric broadening just mentioned. Using the same α parameter and taking into account the in-plane parabolic energy dispersion of the cavity mode, a good description of the data (dash-dotted line) can be obtained assuming a typical lateral size of the thickness fluctuations of $\sim$50 nm, which is probably related to the AlAs-over-GaAs interfaces [24]. We have also performed photoluminescence experiments at 8 K and measured the FWHM of the acoustic cavity fundamental electronic transition to be (3.0 ± 0.4) meV. From calculations in the envelope function approximation, the value of α required to produce this FWHM is 0.05 nm, in very good agreement with the one obtained from Raman scattering.

To summarize, we have shown that the Q factor of THz acoustic cavities can be tailored by design, and that the main present limitation is related to submonolayer thickness fluctuations. Once this extrinsic factors are addressed, these results imply that acoustic cavities with a Q factor as high as 1000 can be grown with MBE technology in the 0.1–1 THz range. We have also found a linear temperature dependence of anharmonic decay, opening the way to fundamental studies of phonon properties in the relevant THz and room-temperature regime.

We thank R. Ouillon and P. Ranson for their assistance with the FP system, L. Largeau and O. Mauguin for the x-ray measurements, and A. Bruchhausen for the core of the simulations program.

*afains@cab.cnea.gov.ar

[1] K.-H. Lin *et al.*, Phys. Rev. B **70**, 073307 (2004).
[2] A. J. Kent *et al.*, Phys. Rev. Lett. **96**, 215504 (2006).
[3] A. Akimov *et al.*, Phys. Rev. Lett. **97**, 037401 (2006).
[4] M. Trigo *et al.*, Phys. Rev. Lett. **89**, 227402 (2002).
[5] K. Sokolowski-Tinten *et al.*, Nature (London) **422**, 287 (2003).
[6] M. F. Pascual Winter *et al.*, Phys. Rev. Lett. **98**, 265501 (2007).
[7] A. Bartels *et al.*, Appl. Phys. Lett. **72**, 2844 (1998).
[8] K. Iga, Jpn. J. Appl. Phys. **47**, 1 (2008).
[9] V. Narayanamurti *et al.*, Phys. Rev. Lett. **43**, 2012 (1979).
[10] A. Huynh *et al.*, Phys. Rev. Lett. **97**, 115502 (2006).
[11] P. G. Klemens, J. Appl. Phys. **38**, 4573 (1967).
[12] C. Herring, Phys. Rev. **95**, 954 (1954).
[13] W. Chen *et al.*, Philos. Mag. B **70**, 687 (1994).
[14] W. S. Capinski *et al.*, Phys. Rev. B **59**, 8105 (1999).
[15] B. C. Daly *et al.*, Phys. Rev. B **66**, 024301 (2002).
[16] C. Ulrich *et al.*, Phys. Rev. Lett. **78**, 1283 (1997).
[17] C. Aku-Leh *et al.*, Phys. Rev. B **71**, 205211 (2005).
[18] J. Kulda *et al.*, Phys. Rev. B **69**, 045209 (2004).
[19] A. Fainstein and B. Jusserand, Phys. Rev. B **57**, 2402 (1998); A. Fainstein *et al.*, Phys. Rev. B **53**, R13287 (1996).
[20] P. Lacharmoise *et al.*, Appl. Phys. Lett. **84**, 3274 (2004).
[21] R. Ouillon *et al.*, Chem. Phys. **91**, 119 (1984).
[22] J. He *et al.*, Phys. Rev. B **37**, 4086 (1988).
[23] P. G. Klemens, Phys. Rev. **122**, 443 (1961).
[24] M. Tanaka *et al.*, Jpn. J. Appl. Phys. **25**, L155 (1986).
[25] T. Ruf *et al.*, Phys. Rev. Lett. **71**, 3035 (1993).